IEEE Photonics Journal
An IEEE Photonics Society Publication

Invited Paper

Quantum Dots for Single- and Entangled-Photon Emitters

Volume 1, Number 1, June 2009

Dieter Bimberg, Senior Member, IEEE
Erik Stock
Anatol Lochmann
Andrei Schliwa
Jan A. Töfflinger
Waldemar Unrau
Michael Münnix
Sven Rodt
Vladimir A. Haisler
Aleksandr I. Toropov
Askhat Bakarov
Aleksandr K. Kalagin

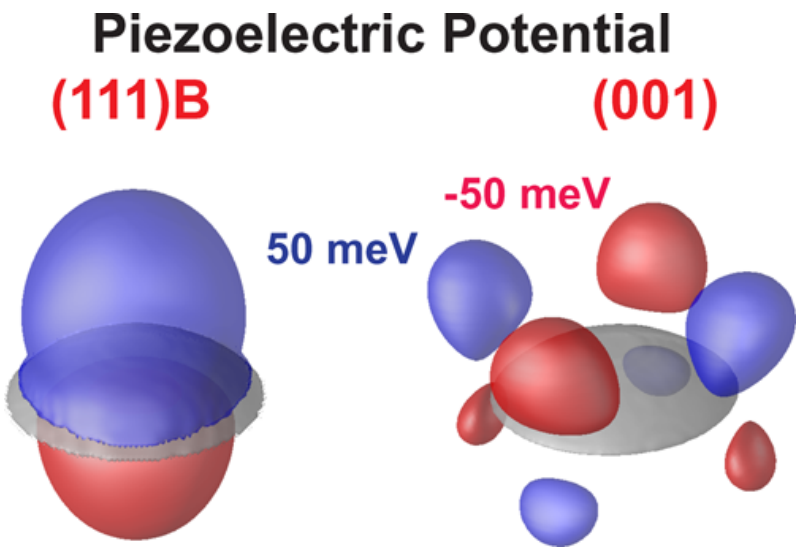

DOI: 10.1109/JPHOT.2009.2025329
1943-0655/$25.00 ©2009 IEEE

Quantum Dots for Single- and Entangled-Photon Emitters

Dieter Bimberg,[1] *Senior Member, IEEE*, Erik Stock,[1] Anatol Lochmann,[1] Andrei Schliwa,[1] Jan A. Töfflinger,[1] Waldemar Unrau,[1] Michael Münnix,[1] Sven Rodt,[1] Vladimir A. Haisler,[2] Aleksandr I. Toropov,[2] Askhat Bakarov,[2] and Aleksandr K. Kalagin[2]

(Invited Paper)

[1]Technische Universität Berlin, Institut für Festkörperphysik, Berlin, Germany
[2]Institute of Semiconductor Physics, Novosibirsk, Russia

DOI: 10.1109/JPHOT.2009.2025329

Manuscript received April 24, 2009; revised May 22, 2009. First published Online June 16, 2009. Current version published July 8, 2009. This work was supported in part by the SFB 787 of DFG and the SfP 982735. V. Haisler acknowledges financial support from DLR/bmbf and TUB. Corresponding author: A. Schliwa (e-mail: andrei.schliwa@googlemail.com).

Abstract: The efficient generation of polarized single or entangled photons is a crucial requirement for the implementation of quantum key distribution (QKD) systems. Self-organized semiconductor quantum dots (QDs) are capable of emitting one polarized photon or an entangled photon pair at a time using appropriate electrical current injection. We realized a highly efficient single-photon source (SPS) based on well-established semiconductor technology: In a pin structure, a single electron and a single hole are funneled into a single InAs QD using a submicron AlO_x current aperture. Efficient radiative recombination leads to emission of single polarized photons with an all-time record purity of the spectrum. Non-classicality of the emitted light without using additional spectral filtering is demonstrated. The out-coupling efficiency and the emission rate are increased by embedding the SPS into a micro-cavity. The design of the micro-cavity is based on detailed modeling to optimize its performance. The resulting resonant single-QD diode is driven at a repetition rate of 1 GHz, exhibiting a second-order correlation function of $g^{(2)}(0) = 0$. Eventually, QDs grown on (111)-oriented substrates are proposed as a source of entangled photon pairs. Intrinsic symmetry-lowering effects leading to the splitting of the exciton bright states are shown to be absent for this substrate orientation. As a result, the $XX \rightarrow X \rightarrow 0$ recombination cascade of a QD can be used for the generation of entangled photons without further tuning of the fine-structure splitting via QD size and/or shape.

Index Terms: Quantum dots (QDs), single-photon emission, entangled photon pairs.

1. Introduction

The strong spatial confinement of electrons and holes on length scales smaller than the de Broglie wavelength in self-organized semiconductor quantum dots (QDs) [1] results in a unique electronic structure with discrete energy levels [2]. Therefore, QDs are often referred to as "artificial atoms in a dielectric cage" [3]. Electron and hole ground states of a QD show only twofold (spin) degeneracy. The recombination is of excitonic character, revealing single excitons, trions and excitonic molecules. The excitonic and biexcitonic emissions are split into polarized doublets caused by e-h exchange interaction. The size of the splitting depends on QD size, shape, chemical composition, and substrate orientation [4]–[6]. Thus, single QDs are the ideal source to generate single q-bits or entangled photons on demand.

Single-QD-based LEDs can be fabricated at low cost using well-established epitaxial and processing techniques [3], [7]. First demonstrations of single-photon sources (SPSs) based on QDs focused on optical pumping [8], [10], [16], [36], [37]. Electrical pumping, however, is by far preferred. No external pump sources are required and electrical triggering of photon emission is easy. Such light sources are required for applications in optical quantum information processing, such as secret key distribution [9], [10] and optical quantum computation [11]. The most immediate application for SPS is the GHz clocked quantum cryptography with demonstrations in free space [12] and in an optical fiber [13].

Electrical pumping of single QDs embedded in pin-diode structures has been attempted recently [14], [15], [17]–[21]. Electrical pumping of the device poses two main challenges: The first is the control of the current path in a way that only one QD is pumped, and the second is to assure that the QD is equally filled by electrons and holes to achieve uncharged excitonic emission. The biexcitonic decay cascade leads to the creation of entangled photon pairs (provided the fine-structure splitting (FSS) is small enough) [22] or for large FSS to the creation of single polarized photons, prerequisite for the BB84 protocol [23].

The first challenge is met by placing a current aperture closely on top of the QDs. The second problem is solved by choosing the proper vertical position of the QD sheet within the pin junction.

The second key for the realization of a quantum cryptography system is a high repetition rate and a low fraction of empty pulses. The repetition rate is limited by the exciton life time and the parasitic electrical bandwidth of the device, whereas the number of empty pulses is mainly controlled by the out-coupling efficiency.

The exciton life time can be reduced and, hence, the emission rate enhanced by placing the optical source inside a cavity, whose dimensions are on the order of the emitted wavelength following the proposal by Purcell [24]. The Purcell effect was observed for QDs in a micro-cavity about 50 years later by Gerard *et al.* [25]. The enhancement of the emission rate, described by the Purcell factor, is determined by geometrical cavity properties alone, such as the quality factor and the effective mode volume. The cavity can be made of Bragg reflectors on top and below the active zone. Given the optical source is in resonance with the cavity dip, not only the emission rate is enhanced, but even more important, the emission becomes directed and the out-coupling efficiency is greatly improved. For optimizing the vertical position, the thickness and the diameter of the current aperture have to be properly designed.

This paper is organized as follows:

Results for single electrically driven q-bit emitters are given in Section 2. Our efforts in optimizing the cavity design are summarized in Section 3, and a resulting high-frequency single-photon emitter is presented in Section 4. Finally, we present the decisive advantages of (111) substrate orientation over the commonly used (001) substrate for entangled-photon emitters in Section 5.

2. Electrically Driven Single-Photon Emitter

A promising approach for SPSs based on electrically driven QDs is the use of a micron-size aluminum-oxide aperture. The aperture can restrict the current such that only one single QD is excited [7], [17], [18]. Selective oxidation of AlGaAs layers with high Al content is used to fabricate the oxide aperture. In this way electrical excitation of more than one dot was significantly suppressed and non-classical light from a single dot is observed. In our device, we funnel only one electron and one hole into one QD. This ultimate control results in an extremely clean spectrum without the need of optical filtering to observe non-classical features of the emitted light.

Fig. 1(a) shows schematically the structure of our device, a pin-diode with submicron oxide current aperture. The pin-diode consists of an undoped GaAs layer with a low-density layer of InAs QDs inserted, the 60-nm-thick aperture layer of high aluminum content AlGaAs/AlO_X, and p- and n-type GaAs electrical contact layers. To minimize the influence of current spreading, the distance between the AlGaAs aperture layer and the InAs QD layer is reduced to only 20 nm. Our structures were grown on semi-insulating (001) epi-ready GaAs substrates using a Riber-32P MBE system. The low density (around 10^8 cm^{-2}) of InAs QDs was obtained by depositing 1.8 ML of InAs. Cylindrical mesas were processed by inductively coupled plasma reactive ion etching. Submicron-size oxide current

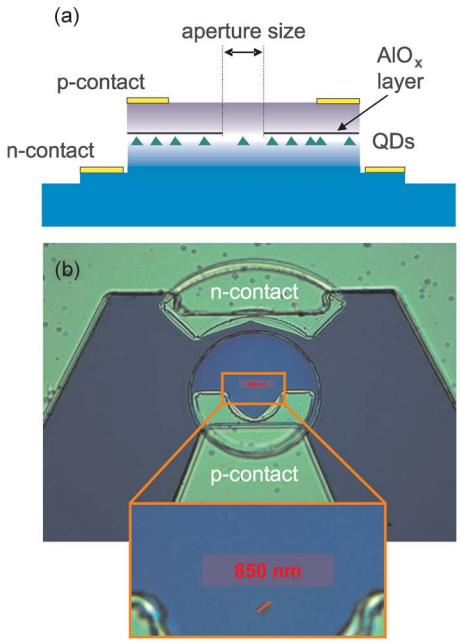

Fig. 1. Schematic figure of the cross section of the investigated single QD emitter (a) and a microscope image of the processed device (b). The inset shows the section with the 0.85-μm oxide aperture.

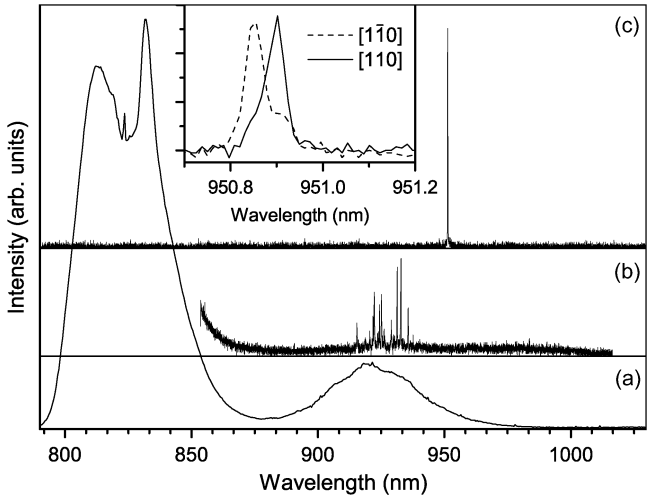

Fig. 2. (a) Macro-photoluminescence of the device shown in Fig. 1. (b) Micro-photoluminescence with a laser spot size of 2 μm. (c) Electroluminescence spectrum at a current of 870 pA and 1.65 V. The inset shows a high-resolution spectrum of the exciton emission line at 0.9 nA. Polarization occurs along the [110] and [$1\bar{1}0$] crystal axes. All spectra are recorded at 15 K.

apertures were created by selective oxidation of the high-aluminum-content aperture AlGaAs layers. Tapering of the oxide current aperture was used to enhance the stability of the oxide structure and to improve the injection characteristics of the QD-LED [15], [26]. The oxidation was performed in an optimized H_2O–N_2 environment at T = 420 °C [26]. After the selective oxidation, Si_3N_4 deposition was performed, followed by Au/Pt/Ti and Au/Au-Ge/Ni metallization to form p- and n-contacts, respectively. Fig. 1(b) shows a microscope image of the processed device. In the middle of the U-shaped p-contact the oxide aperture with a diameter of 0.85 μm is visible.

Fig. 2(a) shows a macro-photoluminescence spectrum, using a frequency doubled Nd:YVO laser emitting at 532 nm at 15 K of the sample. Besides emission from the GaAs bulk material a broad

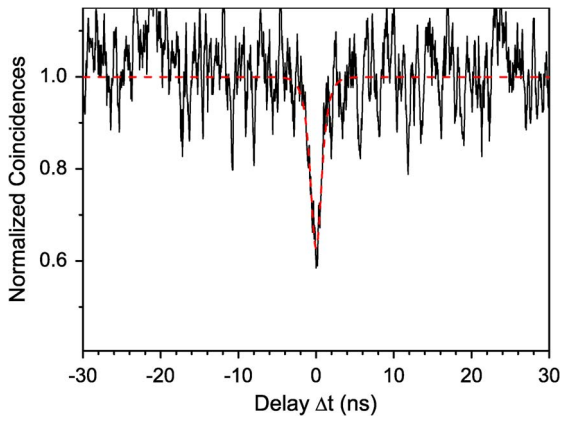

Fig. 3. Photon correlation function measured under continuous-wave current injection (0.9 nA, 1.65 V) at 10 K. No spectral filtering was used to separate the emission of a single QD. The dashed line shows a fit function as described in the text.

emission from the QD ensemble is visible around 925 nm. With a standard micro-photoluminescence setup consisting of a continuous-flow helium cryostat, a 100x microscope objective and a triple monochromator with a spectral resolution of 30 pm FWHM only a few QDs are excited. The broad emission decomposes into a few sharp lines [see Fig. 2(b)].

Finally, the electroluminescence spectrum shown in Fig. 2(c), taken for a current of 870 pA at a bias voltage of 1.65 V, shows an extremely clean spectrum of the emitted light from our device. Only one single line is visible, even emission from the wetting layer or the GaAs bulk material is completely suppressed. At high spectral resolution an FSS of 55 μeV of the emission line into two orthogonally polarized lines is observed (see the inset of Fig. 2). The polarization is directed along the [110] and $[1\bar{1}0]$ crystal axes, thus proving that the light originates from an uncharged QD [27].

As the oxide aperture above the QD is transparent for near infrared light, the absence of other light emission than from the exciton ground state clearly demonstrates, that indeed only a single QD is pumped. This is in contrast to work from other groups where several QDs are pumped and the emission from all QDs except one is blocked by a shadow mask and/or spectral filtering.

The extremely clean spectrum of the QD-LED [see Fig. 2(c)] allows now to detect non-classical features of the emitted light without the need for additional spectral filtering. We used a Hanbury Brown-Twiss (HBT) setup [28] to measure the photon correlation function. In order to avoid cross-talk between the two avalanche photo diodes (APDs) a band pass filter (10 nm FWHM) with a central wavelength of 953 nm was placed in front of one detector.

The normalized photon correlation function under continuous-wave current injection of 0.9 nA is shown in Fig. 3. It shows a clear antibunching dip at zero time delay. Due to the time resolution of the HBT (FWHM = 700 ps) it is not possible to measure the true correlation function $g^{(2)}_{\text{true}}(\Delta t) = 1 - (1 - g^{(2)}_{\text{true}}(0))\exp(-\Delta t/\tau)$. The measured $g^{(2)}_{\text{meas}}(\Delta t)$ is related to the true correlation function via

$$g^{(2)}_{\text{meas}}(\Delta t) = g^{(2)}_{\text{true}}(\Delta t) \otimes \text{Gauss}(\Delta t, \text{FWHM} = 700\ \text{ps}).$$

The dashed red line in Fig. 3 shows a fit of $g^{(2)}_{\text{meas}}(\Delta t)$ to our data resulting in $g^{(2)}_{\text{true}}(0) = 0.3$.

Fig. 4 shows six spectra for increasing injection current. Above 1 nA, the exciton emission intensity saturates, and two additional lines appear. The high-energy line 4 meV below the exciton emission shows the same doublet structure as the exciton line, and its intensity increases superlinearly. Furthermore, both lines show the same spectral jitter, and therefore originate from the same QD [29]. The high-energy line originates from the biexciton. The third emission line between the exciton and biexciton emission is unpolarized and does not show any splitting. We attribute this line to the emission from a charged exciton.

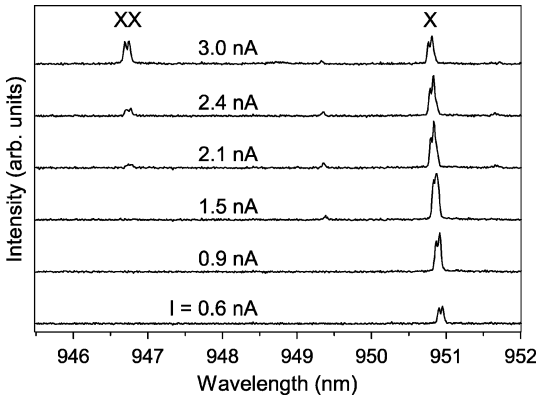

Fig. 4. Electroluminescence spectra for different current injection. For clarity, an offset was added to each spectrum. The exciton emission saturates above 0.9 nA, and the biexciton starts to gain intensity.

The injected current can be adjusted at will, e.g., such that the exciton and biexciton intensities become comparable. Such a situation is ideal for the generation of cascaded photons. The emission from uncharged dots in our device opens the way for generating entangled photon pairs on demand from a QD-LED by reducing the FSS to zero (see Section 5).

Another remarkable feature of our structure is the high conversion efficiency of injected charge carriers into photons. We observed that an injection current of 870 pA corresponding to $\approx$5 electrons/ns is sufficient to saturate the exciton emission. At this point the photon emission rate is limited by the lifetime, which is approximately 1 ns [30]–[32] for an exciton in self-organized QDs grown by MBE. As the capture time of carriers is much shorter (a few picoseconds) we can infer an injection efficiency of about 20%. This is two orders of magnitude improved as compared to the driving current in other structures [14], [15], [17], [18].

3. SPS in a Resonant Cavity

In order to increase the out coupling efficiency and the QD emission rate we developed a Resonant-Cavity LED (RC-LED). Distributed Bragg reflectors (DBRs) at the bottom and on top of the device define a microcavity containing the single electrically driven InAs QD and the AlO_X aperture. The modeling described in this section aims at the determination of optimal position, thickness and diameter of the aperture, as well as the optimal geometry of the QD-aperture-cavity system [33].

Since the diameter of RC-LEDs is large (30–40 μm), compared with a micropost SPS, the oxide aperture is of major importance for the optical field distribution. It serves two main purposes:

1) reduction of the cavity volume, leading to an increase of the photon emission rate due to the Purcell effect;
2) confinement of the radial electromagnetic field and, therefore, directed emission.

The electric-field distribution of a source in any kind of structure with cylindrical symmetry can be calculated by the eigenmode expansion technique [33]. Using this technique the change of spontaneous emission rate can be calculated as function of the wavelength. Not only points of largest resonance, but also regions with suppression of spontaneous emission (Purcell factor, $F_P < 1$) can, thus, be identified.

Since the aperture is used to radially confine the electric field, higher transverse modes are suppressed [34], [35], and only the components of the source emitting close to the direction of the cavity axis will couple to the cavity. For this reason, a horizontally oscillating dipole, which has its emission maximum toward the cavity axis, is a good approximation for a single QD. As the source strength is proportional to the emitted power P and only spontaneous emission occurs, the ratio of the strength of the dipole to its initial strength is proportional to the increase of spontaneous emission rate.

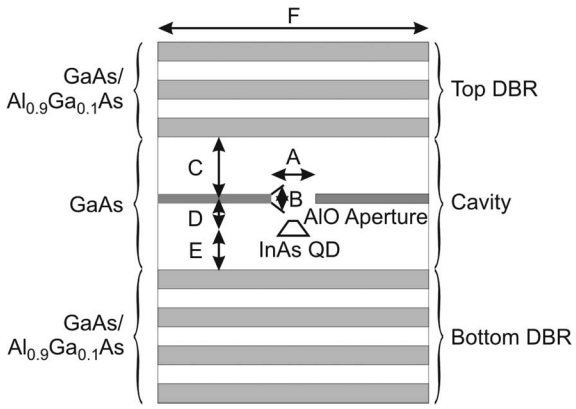

Fig. 5. RC-LED-type SPS. Optimization parameters: A: Aperture diameter, B: Aperture thickness, C: Top DBR-aperture spacing, D: Aperture-QD spacing, E: QD-bottom DBR spacing, F: Mesa diameter.

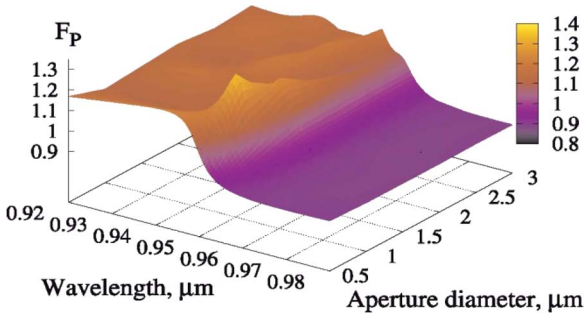

Fig. 6. Purcell factor versus aperture diameter and wavelength for a 20-nm-thick aperture placed at optimal vertical position. The local maxima indicate a reasonable tradeoff between diffraction and confinement of the electromagnetic field due to the aperture.

To calculate the optimal device geometry of an RC-LED-based SPS, the parameters A to F in Fig. 5 have been varied simultaneously. The calculations demonstrate the sensitivity of the Purcell factor to all of the investigated parameters. Fig. 6 shows the resulting Purcell factor if the aperture diameter and the wavelength are varied. The variation with the aperture thickness is strongest for thin apertures, thus, the thickness has been chosen as 20 nm in this calculation. The highest resonance is clearly shown for an aperture diameter of 1 μm (see Fig. 5, Parameter A), because the radial confinement of the electric field is maximal at this point. A further decrease of the diameter reduces the radial confinement due to diffraction.

The enhancement of the spontaneous emission rate is maximal when the electric field is optimally confined by the aperture. This coincides with the lowest possible external emission angle, which can be reduced to approximately 30°. When the aperture parameters are chosen to be outside the tolerances, the confinement of the electromagnetic field and therefore the Purcell factor decrease rapidly. When the cavity is tuned to maximal radial confinement of the electric field, the field vanishes very quickly in the radial direction. Thus, the diameter of the mesa (see Fig. 5, Parameter F) does not affect the change in spontaneous emission.

4. GHz Single-Photon Emitter

Based on the simulations outlined in Section 3, we realized an optimized RC-LED. This device consists of a layer of InAs/GaAs QDs grown by MBE with a density of $5 \cdot 10^8$ cm^{-2} embedded in a pin-diode structure. The current is constricted by an AlO_X aperture which allows pumping of a single QD [7], [18]. These parts of the device are similar to the one from Section 2. In order to increase the out-coupling efficiency and to decrease the exciton lifetime, a microcavity consisting of 12/5 distributed

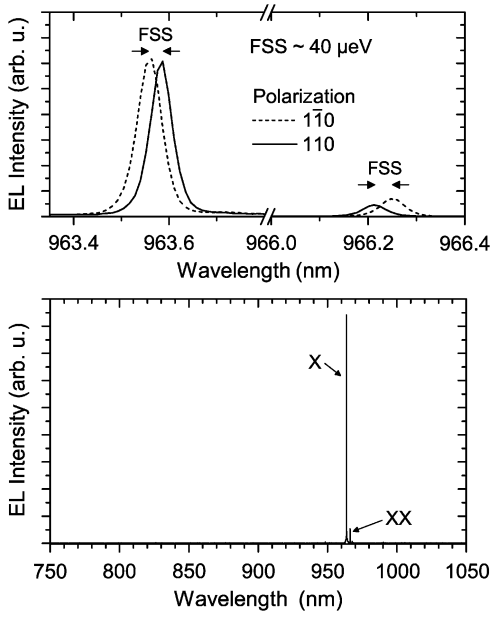

Fig. 7. (Top) High-resolution electroluminescence spectra of X and XX, illustrating the FSS. (Bottom) Overview of the electroluminescence from our RC-LED under pulsed current injection at 15 K. Over a spectral range of 300 nm only the exciton and biexciton lines are visible.

Bragg mirrors on the bottom/top of the device were grown. This yields a micro-cavity Q factor of about 130. Further device processing was carried out as described in Section 2.

The DBR mirrors increase the serial resistance and the capacity of our device in comparison to simpler devices and may reduce the bandwidth and deform the shape of an electrical pulse. Yet we are able to drive our device at a repetition rate of 1 GHz using a pulse width of 350 ps, by increasing the voltage at the pulse generator to 3.1 V. In Fig. 7, the pulsed electroluminescence spectrum of the RC-LED-based SPS at 15 K is shown, being identical to a cw spectrum measured at a bias of 1.5 V and 9 nA. Within the spectral sensitivity of our Si-detector only two emission lines from one single QD are visible. Both lines show a polarization-dependent FSS of around 40 μeV, identifying these two lines as exciton and biexciton emission line. The emission of polarized photons makes it possible to use such a device for entangled photon pairs by reducing the FSS to zero [22], as described in Section 5.

The count rate of our APDs is more than twenty times higher than from previous devices shown in Section 2 [7] without cavity, proving the higher spontaneous emission rate, and in the first place, the increased out-coupling efficiency of our device.

In order to investigate the maximum repetition rate we used the trigger signal of the pulse generator as start signal and one APD as stop signal for time-correlated measurements. The measured optical response (see Fig. 8, top) agrees very well with theoretical simulations for a pulse train with a FWHM of 400 ps (red line). The temporal resolution of our APD is 350 ps, thus presently still limiting the measured optical response. The exciton life time without cavity is in the order of 1 ns and the short optical response of our device demonstrates an appreciable reduction of the lifetime by at least a factor of two, due to the Purcell effect. This result is in excellent agreement with our simulations shown in Section 3.

For photon correlation measurements two APDs for the start and stop signal must be used, thus reducing the time resolution by the factor of 2. With this time resolution it is not possible to resolve the 400 ps pulses of our device and the measured correlation function (see Fig. 8, bottom) looks similar to cw excitation. As described in Section 2, the measured $g^{(2)}(0)$ value is again limited by the time resolution of our setup. The photon correlation agrees excellently with a simulation (see the red line in Fig. 8) for a pulsed perfect single-photon device $(g^{(2)}(0) = 0)$ with 1 GHz repetition rate, taking into account the limited time resolution of 0.7 ns of our setup.

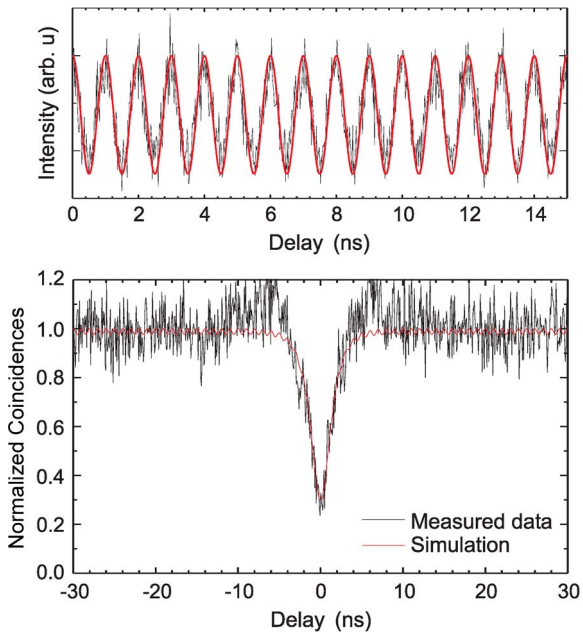

Fig. 8. (Top) Optical response of our device to an electrical 1-GHz signal with a pulse width of 350 ps and simulation of a pulse train with 400 ps width (red line). (Bottom) Correlation measurement at the same frequency demonstrates clear antibunching. The red line is a simulation of a pulsed perfect single-photon device $(g^{(2)}(0) = 0)$ with 1-GHz repetition rate, taking into account the limited time resolution of 0.7 ns of the setup.

5. QDs on (111) Substrate for Entangled Photon Pairs

The most promising proposal for the creation of entangled photon pairs in QD-based sources relies on the biexciton $(XX) \rightarrow$ exciton $(X) \rightarrow 0$ recombination cascade [22]. A vanishing FSS of the exciton bright state is essential in order to achieve entanglement [36], [37]. For QDs grown on (001) substrates, a zero FSS is hard to achieve, because piezoelectricity, interface and strain asymmetries, or even a modest QD elongation induce a lateral anisotropy leading to sizable values of the FSS [4]. Recent advances to reduce the FSS for each QD individually by post-growth techniques like thermal [5] or laser [38] annealing are inefficient, expensive and hardly applicable on an industrial scale.

Structural QD anisotropies originate from different surface mobilities along [110] and $[1\bar{1}0]$, [39] which are tied to the orientation of the underlying zinc-blende lattice with respect to the (001) substrate. Moreover, piezoelectric fields [40]–[42] strain and interface anisotropies arise. This leads to a reduction of the carrier confinement symmetry to C_{2v} or lower [43] and is an intrinsic characteristic of the (001) substrate orientation.

Therefore, we proposed to abandon this orientation and turn to the (111) substrate for QD growth. None of the above-mentioned effects arises on this surface. From the investigations in Refs. [44], [45] we expect a threefold rotational symmetry of the QD structure. The corresponding piezoelectric fields do not lower this symmetry any further. In effect the excitonic bright states remain degenerate and an intrinsically perfect source of entangled photon pairs is available. This result is of general character for this surface and applies to all self-organized QDs in zinc-blende systems. Using eight-band $\mathbf{k} \cdot \mathbf{p}$ calculations in conjunction with the configuration-interaction (CI) method [46], [47], this result is illustrated by comparing the piezoelectric fields and excitonic properties for lens-shaped QDs grown on the (001) and the (111) substrate.

To analyze the impact of the substrate orientations on the piezoelectric potential (Fig. 9) lens-shaped QDs are chosen as model system. For (111) grown QDs, the potential shows C_{3v}-symmetry and a strong gradient along the growth direction, in contrast to (001) grown counterparts, with only C_{2v} in-plane symmetry and no significant potential drop along the [001] axis. The field distribution of the

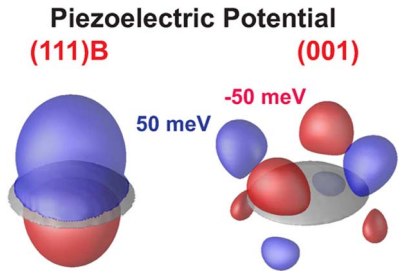

Fig. 9. Comparison of the piezoelectric potentials for lens-shaped QDs (gray) grown on (111)B substrate to those grown on (001). Isosurfaces are shown for values of 50 meV (blue) and −50 meV (red), respectively.

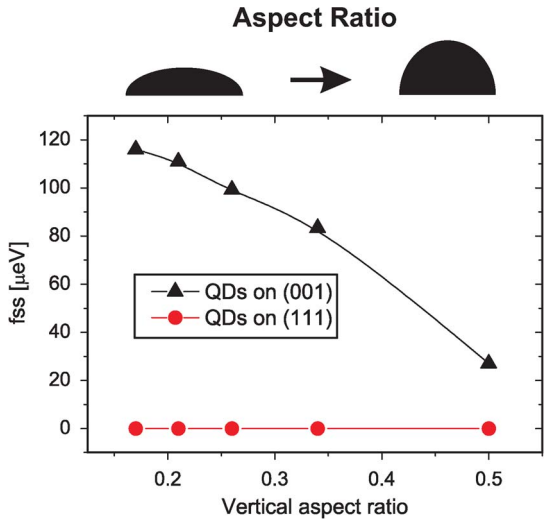

Fig. 10. Exciton bright splitting as function of vertical aspect ratio for lens-shaped InAs/GaAs QDs.

(111) grown QD is similar to the one of *c*-plane wurtzite-type GaN/AlN or InN/GaN QDs [48]–[50]. The magnitude of the potential drop, however, is much larger for the nitride QDs and the field is additionally superposed by pyroelectric effects, which do not occur in zinc-blende crystals.

The few-particle properties such as FSS and biexciton binding energies are calculated using the configuration interaction model [46] taking into account direct Coulomb interaction, exchange (including dipole-dipole terms [51]) and large parts of correlation effects. In Fig. 10, the calculated values of the FSS as function of the QD's vertical aspect ratio are compared between the two substrate orientations (001) and (111). For the (001) QDs an FSS between 120 and 30 μeV is found due to the symmetry breaking effect of piezoelectricity. By contrast the (111) QDs exhibit no FSS at all as expected from our symmetry considerations.

Symmetry lowering effects due to the atomistic nature of the QD interface and such atomistic symmetry anisotropies that are not included via piezoelectricity are not part of our model. For the (111) QDs, however, such effects are not expected to lower the symmetry below C_{3v}. Hence, the FSS still remains zero for (111) QDs. Only random alloying effects within the QD for InGaAs(111) QDs might lead to a deviation from zero FSS.

6. Conclusion

Single-QD LEDs, which include an appropriately placed and sized submicron oxide aperture close to a low-density InAs QD layer allow to inject a single hole and a single electron into a single QD with high efficiency. In this sense a single-QD LED is the ultimate limit for an LED. Excitonic

emission from QDs allows the extraction of single photons with a well-defined polarization state. Inserting the QD in an RC-LED repetition rates of 1 GHz and a $g^{(2)}(0) = 0$ are demonstrated. If the FSS is tuned to zero by QD growth on (111) planes, entangled-photon-pair emission from an electrically pumped device is feasible. Together with the extreme spectral purity such an LED has the potential as an efficient ready-to-go SPS/entangled-photon source for future applications in optical quantum information processing.

Acknowledgment

The calculations were performed on a SGI supercomputer at the HLRN Berlin/Hannover.

References

[1] D. Bimberg, M. Grundmann, and N. N. Ledentsov, *Quantum Dot Heterostructures*. Chichester, U.K.: Wiley, 1998.
[2] O. Stier, M. Grundmann, and D. Bimberg, "Electronic and optical properties of strained quantum dots modeled by 8-band k.p theory," *Phys. Rev. B, Condens. Matter*, vol. 59, no. 8, pp. 5688–5701, Feb. 1999.
[3] D. Bimberg, "Quantum dot based nanophotonics and nanoelectronics," *Electron. Lett.*, vol. 44, no. 3, pp. 168–171, Jan. 2008.
[4] R. Seguin, A. Schliwa, S. Rodt, K. Pötschke, U. W. Pohl, and D. Bimberg, "Size-dependent fine-structure splitting in self-organized InAs/GaAs quantum dots," *Phys. Rev. Lett.*, vol. 95, no. 25, p. 257 402, Dec. 2005.
[5] R. Seguin, A. Schliwa, T. D. Germann, S. Rodt, K. Pötschke, A. Strittmatter, U. W. Pohl, D. Bimberg, M. Winkelnkemper, T. Hammerschmidt, and P. Kratzer, "Control of fine-structure splitting and excitonic binding energies in selected individual InAs/GaAs quantum dots," *Appl. Phys. Lett.*, vol. 89, no. 26, p. 263 109, Dec. 2006.
[6] A. Schliwa, M. Winkelnkemper, and D. Bimberg, "Generation of entangled photon pairs using QDs grown on (111)-zinc-blende substrate," Deutsche Patentanmeldung Nr.: 10 2008 036 400.2, Aug. 1, 2008.
[7] A. Lochmann, E. Stock, O. Schulz, F. Hopfer, D. Bimberg, V. A. Haisler, A. I. Toropov, A. K. Bakarov, and A. K. Kalagin, "Electrically driven single quantum dot polarised single photon emitter," *Electron. Lett.*, vol. 42, no. 13, pp. 774–775, Jun. 2006.
[8] A. J. Bennett, D. C. Unitt, P. Atkinson, D. A. Ritchie, and A. J. Shields, "High performance single photon sources from photolithographically defined pillar microcavities," *Opt. Express*, vol. 13, no. 1, pp. 50–55, Jan. 2005.
[9] N. Gisin, G. Ribordy, W. Tittel, and H. Zbinden, "Quantum cryptography," *Rev. Mod. Phys.*, vol. 74, no. 1, pp. 145–195, Jan. 2002.
[10] T. Aichele, G. Reinaudi, and O. Benson, "Separating cascaded photons from a single quantum dot: Demonstration of multiplexed quantum cryptography," *Phys. Rev. B, Condens. Matter*, vol. 70, no. 23, p. 235 329, Dec. 2004.
[11] M. Scholz, T. Aichele, S. Ramelow, and O. Benson, "Deutsch-Jozsa algorithm using triggered single photons from a single quantum dot," *Phys. Rev. Lett.*, vol. 96, no. 18, p. 180 501, May 2006.
[12] J. Bienfang, A. Gross, A. Mink, B. Hershman, A. Nakassis, X. Tang, R. Lu, D. Su, C. Clark, C. Williams, E. Hagley, and J. Wen, "Quantum key distribution with 1.25 Gbps clock synchronization," *Opt. Express*, vol. 12, no. 9, pp. 2011–2016, May 2004.
[13] K. Gordon, V. Fernandez, P. Townsend, and G. Buller, "A short wavelength GigaHertz clocked fiber-optic quantum key distribution system," *IEEE J. Quantum Electron.*, vol. 40, no. 7, pp. 900–908, Jul. 2004.
[14] Z. Yuan, B. Kardynal, R. M. Stevenson, A. J. Shields, C. Lobo, K. Cooper, N. S. Beattie, D. A. Ritchie, and M. Pepper, "Electrically driven single-photon source," *Science*, vol. 295, no. 5552, pp. 102–105, Jan. 2002.
[15] A. Fiore, J. X. Chen, and M. Ilegems, "Scaling quantum-dot light-emitting diodes to submicrometer sizes," *Appl. Phys. Lett.*, vol. 81, no. 10, pp. 1756–1758, Sep. 2002.
[16] V. Zwiller, T. Aichele, W. Seifert, J. Persson, and O. Benson, "Generating visible single photons on demand with single InP quantum dots," *Appl. Phys. Lett.*, vol. 82, no. 10, pp. 1509–1511, Mar. 2003.
[17] C. Zinoni, B. Alloing, C. Paranthoen, and A. Fiore, "Three-dimensional wavelength-scale confinement in quantum dot microcavity light-emitting diodes," *Appl. Phys. Lett.*, vol. 85, no. 12, pp. 2178–2180, Sep. 2004.
[18] D. J. P. Ellis, A. J. Bennett, A. J. Shields, P. Atkinson, and D. A. Ritchie, "Electrically addressing a single self-assembled quantum dot," *Appl. Phys. Lett.*, vol. 88, no. 13, p. 133 509, Mar. 2006.
[19] R. Schmidt, U. Scholz, M. Vitzethum, R. Fix, C. Metzner, P. Kailuweit, D. Reuter, A. Wieck, M. C. Hübner, S. Stufler, A. Zrenner, S. Malzer, and G. H. Döhler, "Fabrication of genuine single-quantum-dot light-emitting diodes," *Appl. Phys. Lett.*, vol. 88, no. 12, p. 121 115, Mar. 2006.
[20] A. Shields, "Semiconductor quantum light sources," *Nat. Photon.*, vol. 1, no. 4, pp. 215–223, 2007.
[21] X. M. Dou, X. Y. Chang, B. Q. Sun, Y. H. Xiong, Z. C. Niu, S. S. Huang, H. Q. Ni, Y. Du, and J. B. Xia, "Single-photon-emitting diode at liquid nitrogen temperature," *Appl. Phys. Lett.*, vol. 93, no. 10, p. 101 107, Sep. 2008.
[22] O. Benson, C. Santori, M. Pelton, and Y. Yamamoto, "Regulated and entangled photons from a single quantum dot," *Phys. Rev. Lett.*, vol. 84, no. 11, pp. 2513–2516, Mar. 2000.
[23] C. H. Bennett and G. Brassard, "Quantum Cryptography: Public key distribution and coin tossing," in *Proc. IEEE Int. Conf. Comput., Syst., Signal Process.*, 1984, p. 175.
[24] E. M. Purcell, H. C. Torrey, and R. V. Pound, "Resonance absorption by nuclear magnetic moments in a solid," *Phys. Rev.*, vol. 69, no. 1/2, pp. 37–38, Jan. 1946.
[25] J. M. Gerard, B. Sermage, B. Gayral, B. Legrand, E. Costard, and V. Thierry-Mieg, "Enhanced spontaneous emission by quantum boxes in a monolithic optical microcavity," *Phys. Rev. Lett.*, vol. 81, no. 5, pp. 1110–1113, Aug. 1998.

[26] V. A. Haisler, F. Hopfer, R. L. Sellin, A. Lochmann, K. Fleischer, N. Esser, W. Richter, N. N. Ledentsov, D. Bimberg, C. Möller, and N. Grote, "Micro-raman studies of vertical-cavity surface-emitting lasers with Al(x)O(y)/GaAs distributed Bragg reflectors," *Appl. Phys. Lett.*, vol. 81, no. 14, pp. 2544–2546, 2002.
[27] M. Bayer, G. Ortner, O. Stern, A. Kuther, A. A. Gorbunov, A. Forchel, P. Hawrylak, S. Fafard, K. Hinzer, T. L. Reinecke, S. N. Walck, J. P. Reithmaier, F. Klopf, and F. Schäfer, "Fine structure of neutral and charged excitons in self-assembled In(Ga)As/(Al)GaAs quantum dots," *Phys. Rev. B, Condens. Matter Mater. Phys.*, vol. 65, no. 19, p. 195 315, May 2002.
[28] R. H. Brown and R. Q. Twiss, "A test of a new type of stellar interferometer on sirius," *Nature*, vol. 178, no. 4541, pp. 1046–1048, Nov. 1956.
[29] V. Türck, S. Rodt, O. Stier, R. Heitz, R. Engelhardt, U. Pohl, D. Bimberg, and R. Steingrüber, "Effect of random field fluctuations on excitonic transitions of individual CdSe quantum dots," *Phys. Rev. B, Condens. Matter*, vol. 61, no. 15, pp. 9944–9947, Apr. 2000.
[30] R. Heitz, A. Kalburge, Q. Xie, M. Grundmann, P. Chen, A. Hoffmann, A. Madhukar, and D. Bimberg, "Excited states and energy relaxation in stacked InAs/GaAs quantum dots," *Phys. Rev. B, Condens. Matter*, vol. 57, no. 15, pp. 9050–9060, Apr. 1998.
[31] R. M. Thompson, R. M. Stevenson, A. J. Shields, I. Farrer, C. J. Lobo, D. A. Ritchie, M. L. Leadbeater, and M. Pepper, "Single-photon emission from exciton complexes in individual quantum dots," *Phys. Rev. B, Condens. Matter*, vol. 64, no. 20, p. 201 302, Nov. 2001.
[32] P. Michler, *Single Quantum Dots*. Berlin, Germany: Springer-Verlag, 2003.
[33] M. Münnix, A. Lochmann, and D. Bimberg, "Modeling highly efficient RCLED-type quantum dot based single photon emitter," *IEEE J. Quantum Electron.*, 2009, to be published.
[34] F. Hopfer, I. Kaiander, A. Lochmann, A. Mutig, S. Bognar, M. Kuntz, U. W. Pohl, V. A. Haisler, and D. Bimberg, "Vertical-cavity surface emitting quantum-dot laser with low threshold current grown by metalorganic vapor phase epitaxy," *Appl. Phys. Lett.*, vol. 89, no. 6, p. 061105, Aug. 2006.
[35] E. Söderberg, J. S. Gustavsson, P. Modh, A. Larsson, Z. Zhang, J. Berggren, and M. Hammar, "Suppression of higher order transverse and oxide modes in 1.3-μm InGaAs VCSELs by an inverted surface relief," *IEEE Photon. Technol. Lett.*, vol. 19, no. 5, pp. 327–329, Mar. 2007.
[36] N. Akopian, N. H. Lindner, E. Poem, Y. Berlatzky, J. Avron, D. Gershoni, B. D. Gerardot, and P. M. Petroff, "Entangled photon pairs from semiconductor quantum dots," *Phys. Rev. Lett.*, vol. 96, no. 13, p. 130 501, Apr. 2006.
[37] R. M. Stevenson, R. J. Young, P. Atkinson, K. Cooper, D. A. Ritchie, and A. J. Shields, "A semiconductor source of triggered entangled photon pairs," *Nature*, vol. 439, no. 7073, pp. 179–182, Jan. 2006.
[38] A. Rastelli, A. Ulhaq, S. Kiravittaya, L. Wang, A. Zrenner, and O. Schmidt, "In situ laser microprocessing of single self-assembled quantum dots and optical microcavities," *Appl. Phys. Lett.*, vol. 90, no. 7, p. 073120, Feb. 2007.
[39] A. Kley, P. Ruggerone, and M. Scheffler, "Novel diffusion mechanism on the GaAs (001) surface: The role of adatom-dimer interaction," *Phys. Rev. Lett.*, vol. 79, no. 26, pp. 5278–5281, Dec. 1997.
[40] M. Grundmann, O. Stier, and D. Bimberg, "InAs/GaAs pyramidal quantum dots: Strain distribution, optical phonons, and electronic structure," *Phys. Rev. B, Condens. Matter*, vol. 52, no. 16, pp. 11 969–11 981, Oct. 1995.
[41] G. Bester, A. Zunger, X. Wu, and D. Vanderbilt, "Effects of linear and nonlinear piezoelectricity on the electronic properties of InAs/GaAs quantum dots," *Phys. Rev. B, Condens. Matter*, vol. 74, no. 8, p. 081305, Aug. 2006.
[42] A. Schliwa, M. Winkelnkemper, and D. Bimberg, "Impact of size, shape, and composition on piezoelectric effects and electronic properties of In(Ga)As/GaAs quantum dots," *Phys. Rev. B, Condens. Matter*, vol. 76, no. 20, p. 205 324, Nov. 2007.
[43] E. Siebert, T. Warming, A. Schliwa, E. Stock, M. Winkelnkemper, S. Rodt, and D. Bimberg, "Spectroscopic access to single hole energies in InAs/GaAs quantum dots," *Phys. Rev. B, Condens. Matter*, vol. 79, no. 20, p. 205 321, May 2009.
[44] C. Lobo and R. Leon, "InGaAs island shapes and adatom migration behavior on (100), (110), (111), and (311) GaAs surfaces," *J. Appl. Phys.*, vol. 83, no. 8, pp. 4168–4172, Apr. 1998.
[45] Y. Sugiyama, Y. Sakuma, S. Muto, and N. Yokoyama, "Novel InGaAs/GaAs quantum dot structures formed in tetrahedral-shaped recesses on (111) B GaAs substrate using metalorganic vapor phase epitaxy," *Appl. Phys. Lett.*, vol. 67, no. 2, pp. 256–258, Jul. 1995.
[46] M. Brasken, M. Lindberg, D. Sundholm, and J. Olsen, "Full configuration interaction calculations of electron-hole correlation effects in strain-induced quantum dots," *Phys. Rev. B, Condens. Matter*, vol. 61, no. 11, pp. 7652–7655, Mar. 2000.
[47] A. Schliwa, M. Winkelnkemper, and D. Bimberg, "Few-particle energies versus geometry and composition of InGaAs/GaAs self-organized quantum dots," *Phys. Rev. B, Condens. Matter*, vol. 79, no. 7, p. 075443, Feb. 2009.
[48] A. D. Andreev and E. P. O'Reilly, "Optical transitions and radiative lifetime in GaN/AlN self-organized quantum dots," *Appl. Phys. Lett.*, vol. 79, no. 4, pp. 521–523, Jul. 2001.
[49] M. Winkelnkemper, A. Schliwa, and D. Bimberg, "Interrelation of structural and electronic properties in In(x)Ga(1-x)N/GaN quantum dots using an eight-band k · p model," *Phys. Rev. B, Condens. Matter*, vol. 74, no. 15, p. 155 322, Oct. 2006.
[50] M. Povolotskyi, A. D. Carlo, and S. Birner, "Electronic and optical properties of [N11] grown nanostructures," *Phys. Stat. Sol. (C)*, vol. 1, no. 6, pp. 1511–1521, Apr. 2004.
[51] T. Takagahara, "Theory of exciton doublet structures and polarization relaxation in single quantum dots," *Phys. Rev. B, Condens. Matter*, vol. 62, no. 24, pp. 16 840–16 855, Dec. 2000.